Supporting Information

For

Metal-Coordination Driven Intramolecular Twisting: A turn-on Fluorescent-Redox Probe for Hg^{2+} Ion Through Interaction of Ferrocene Nonbonding Orbital and Dibenzylidenehydrazine

Sushil Ranjan Bhatta[a], Bijan Mondal[b‡], Sudhir Lima[c‡] and Arunabha Thakur[a*]

[a]Department of Chemistry, Jadavpur University, Kolkata-700032, India.

[b]Department of Chemistry, Indian Institute of Technology Madras, Chennai-36, India.

[c]Department of Chemistry, National Institute of Technology Rourkela, Odisha-769008, India.

Phone: *033-2457-2779, +919937760940*

Email: arunabha.thakur@jadavpuruniversity.in, babuiitm07@gmail.com

Table of content

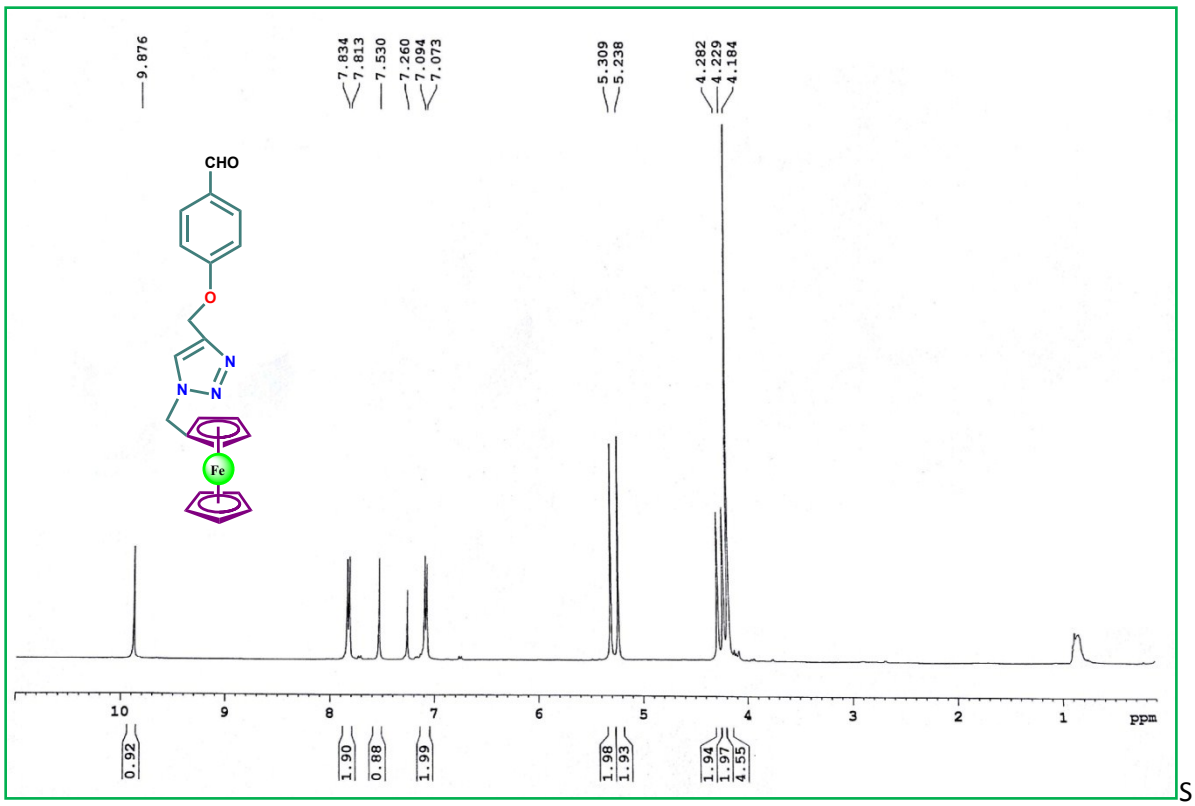

Fig. S1. ^{1}H NMR spectrum of compound **3** in $CDCl_3$ as a solvent.

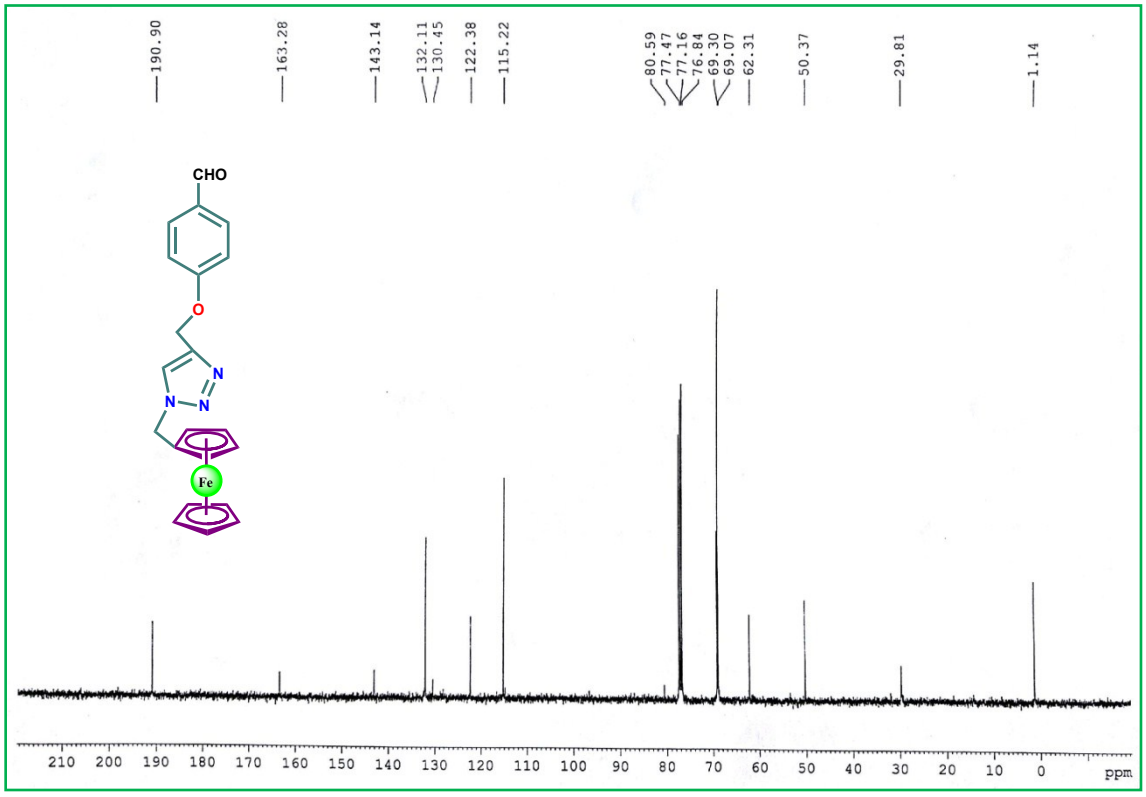

Fig. S2. ^{13}C NMR spectrum of compound **3** in $CDCl_3$ as a solvent.

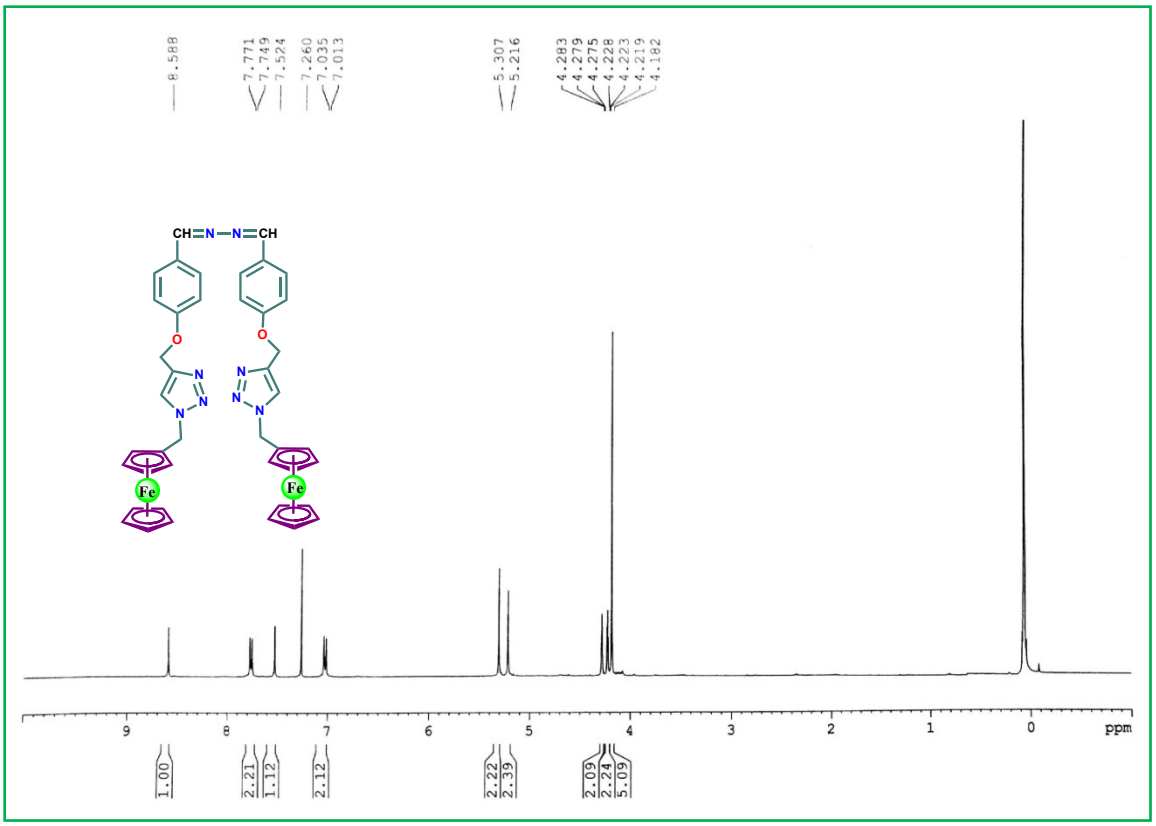

Fig. S3. ^{1}H NMR spectrum of compound **4** in $CDCl_3$ as a solvent.

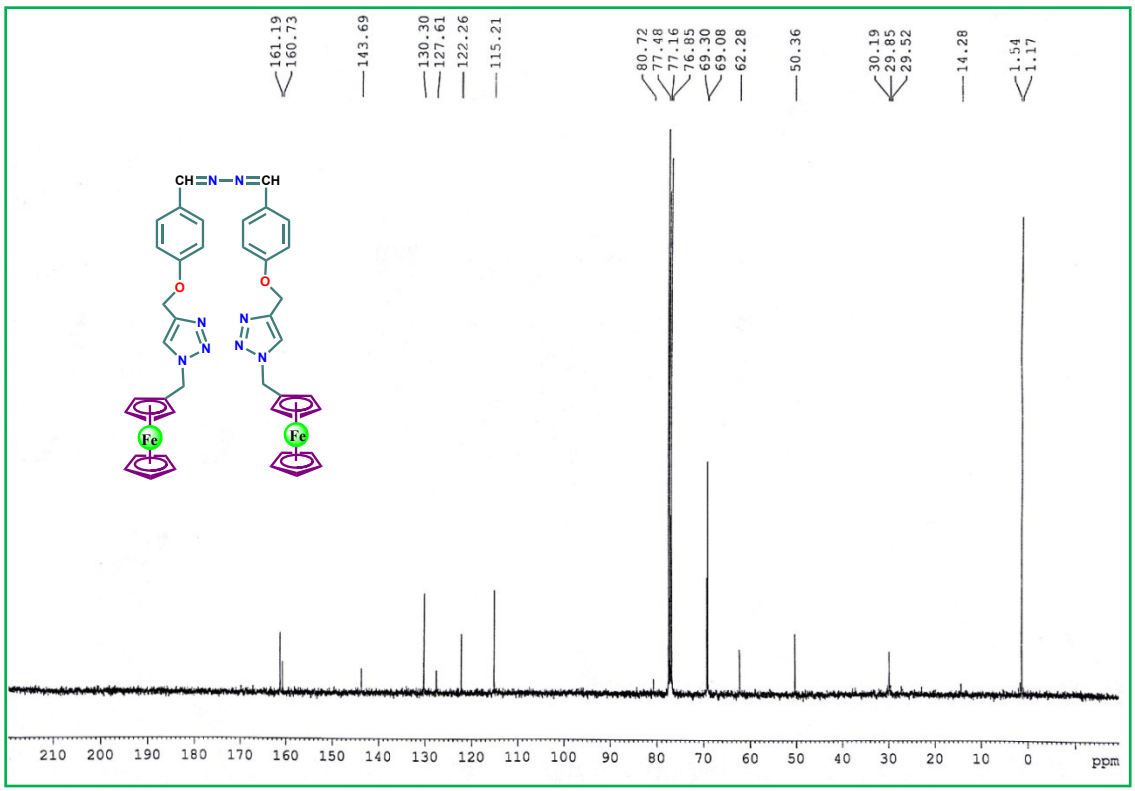

Fig. S4. ^{13}C NMR spectrum of compound **4** in $CDCl_3$ as a solvent.

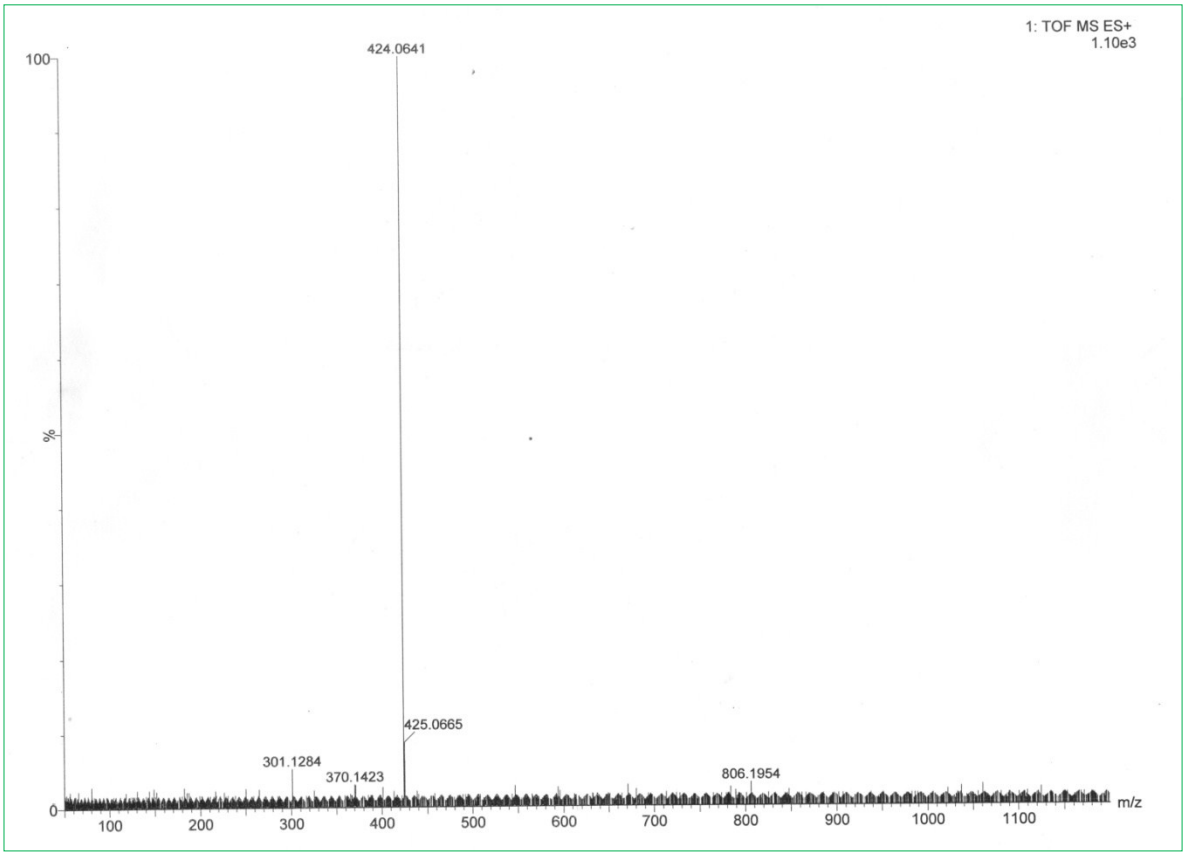

Fig. S5. HRMS spectrum of compound **3**.

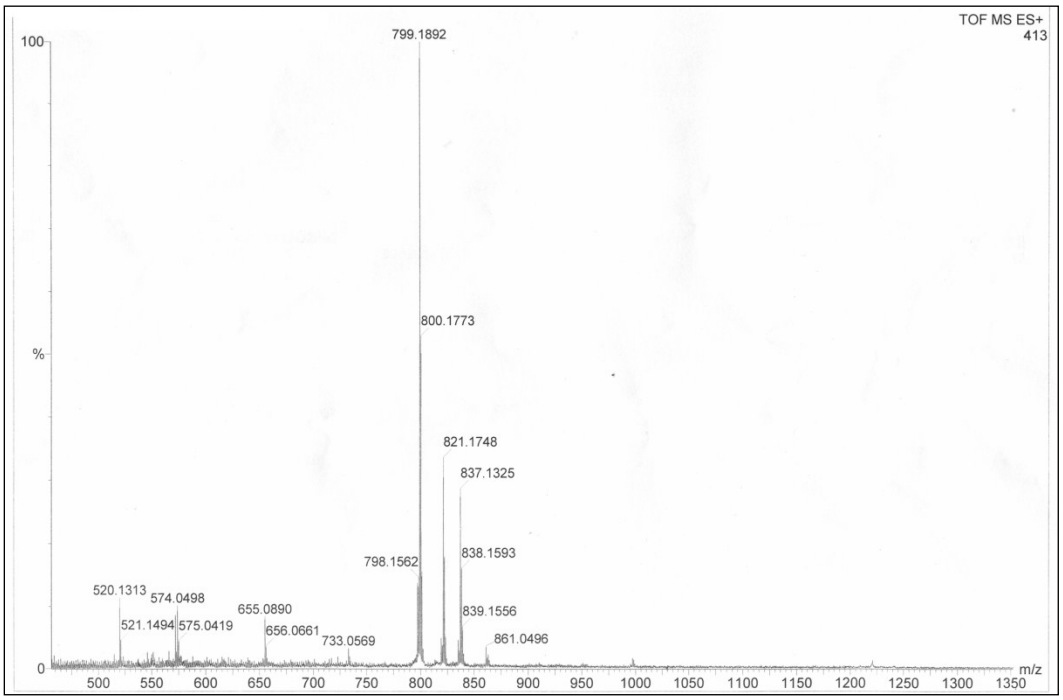

Fig. S6. HRMS spectrum of compound **4**.

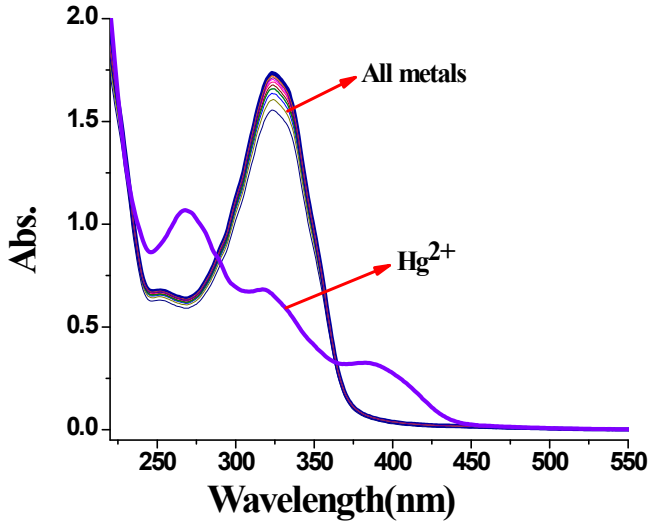

Fig. S7. Changes in the absorption spectra of **4** (10^{-4} M) in CH_3CN/H_2O upon addition of several metal cations tested.

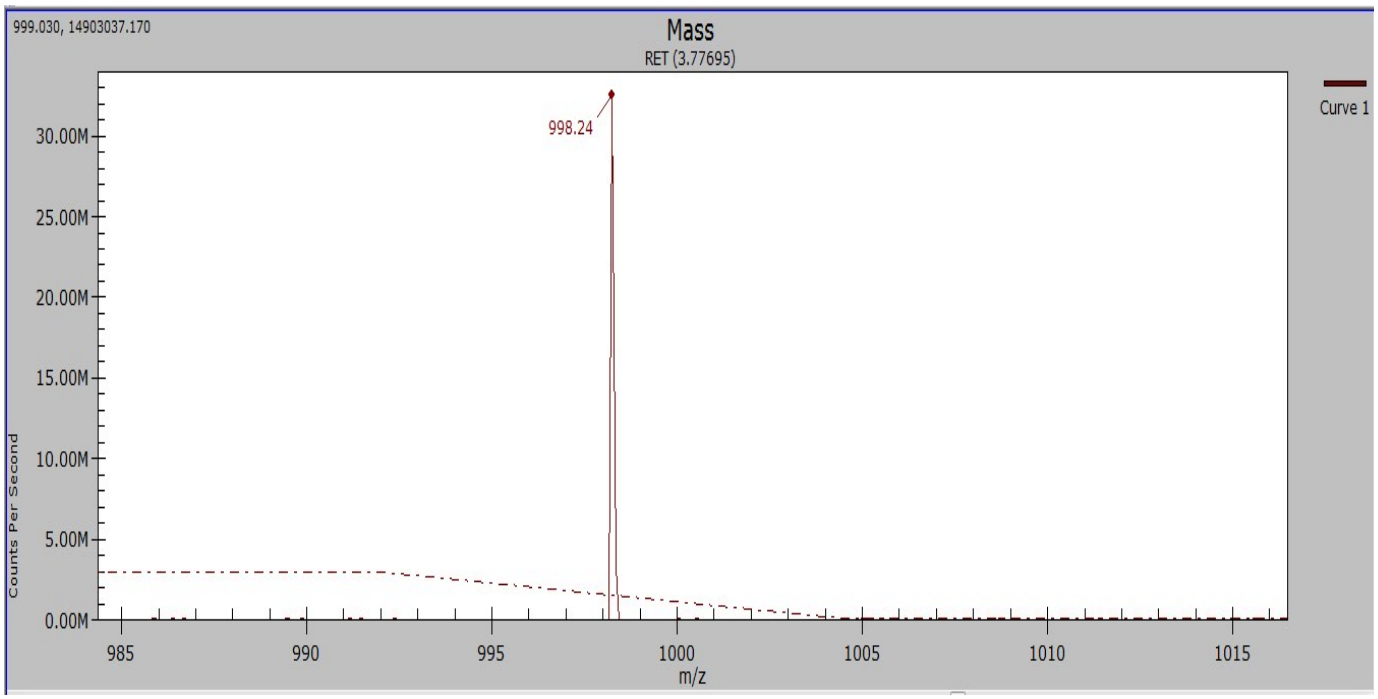

Fig. S8. ESI-mass spectrum of [**4**·Hg^{2+}].

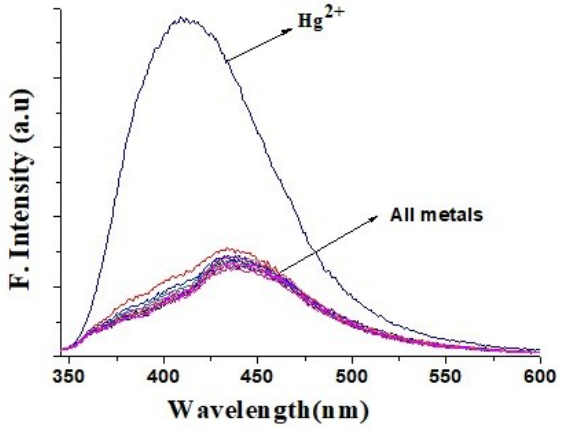

Fig. S9. Effect of adding various metal ions on fluorescence of **4**. $[M^{n+}] = 10^{-6}$ M.

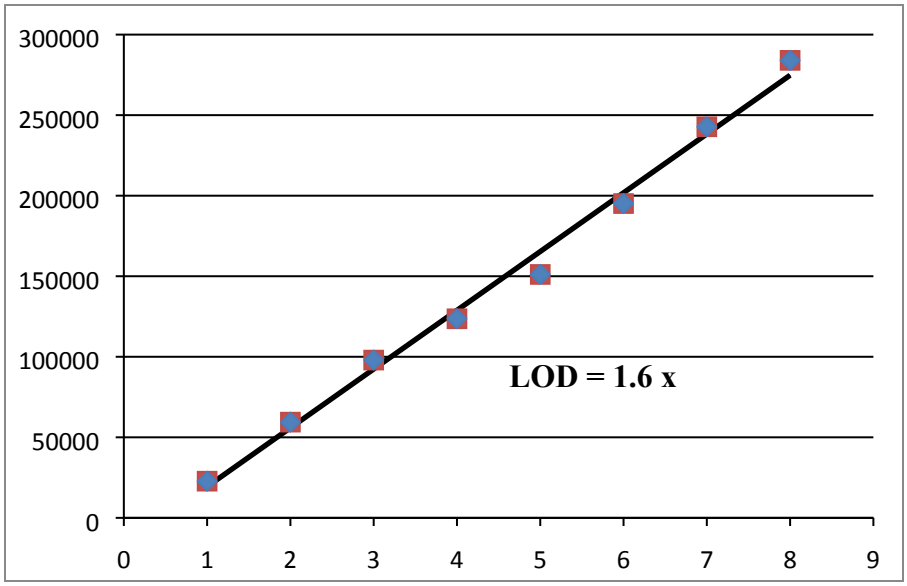

Fig. S10. Calculation of limit of detection (LOD) by 3σ/S method.

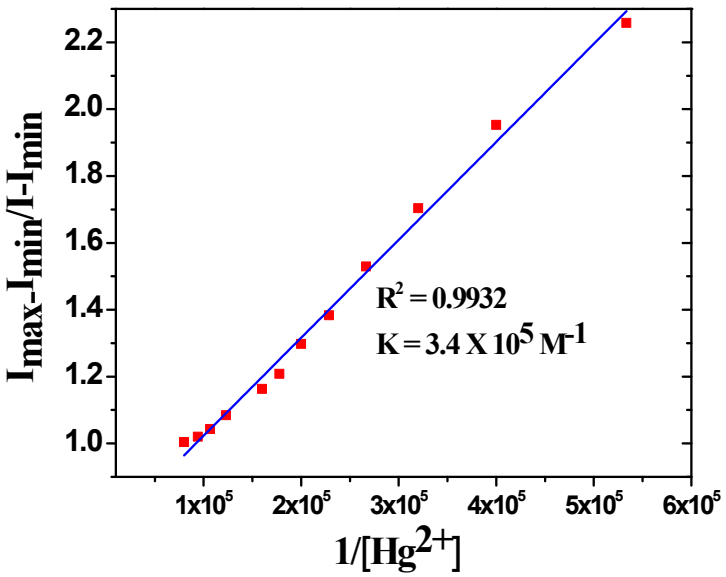

Fig. S11. Quantitative binding data (Benesi-Hildebrand plot) with Hg^{2+} ion.

a)

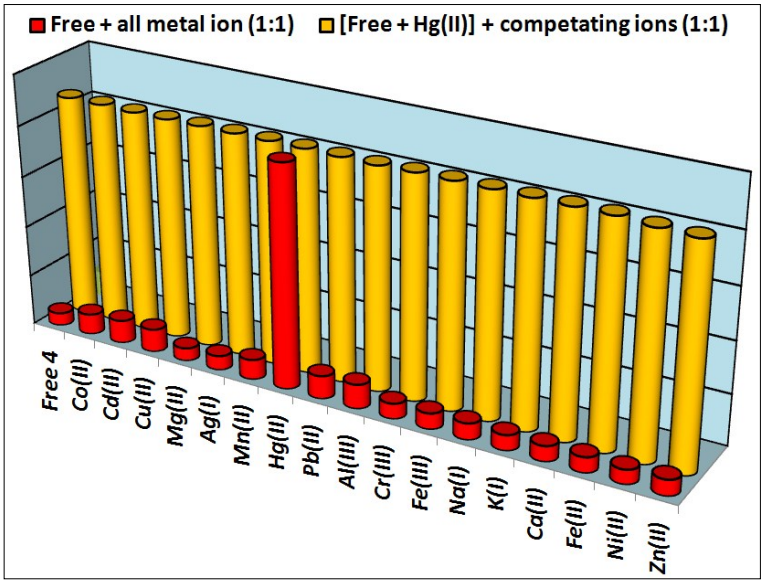

b)

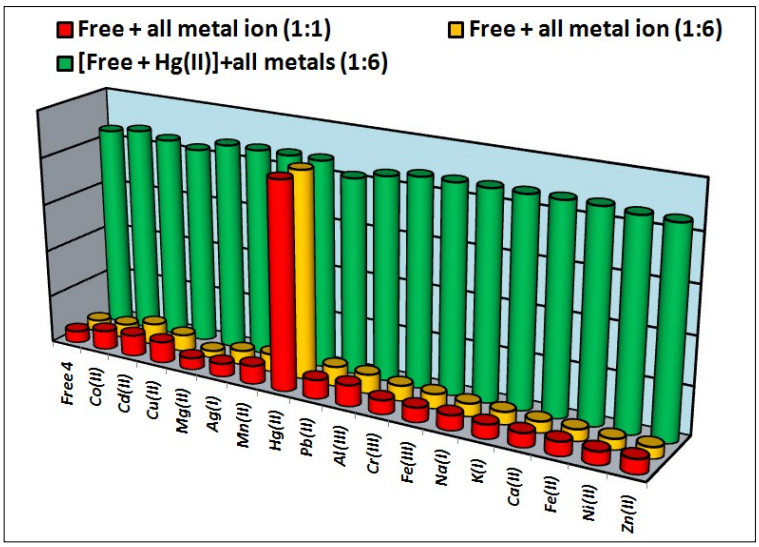

Fig. S12. Bar plot representation of the fluorescence emission intensity of **4** upon the addition of (a) 1 equiv and (b) 6 equiv of several competitive ions in CH_3CN solution.

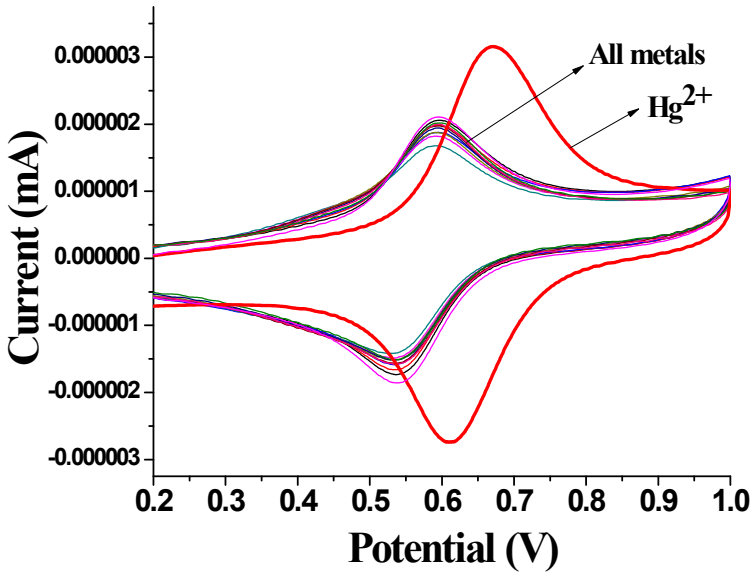

Fig. S13. Evolution of CV of **4** (10^{-4} M) (CH_3CN/H_2O) upon addition of several metal cations in CH_3CN/H_2O (2/8) $[(n\text{-}Bu)_4N]ClO_4$ as supporting electrolyte.

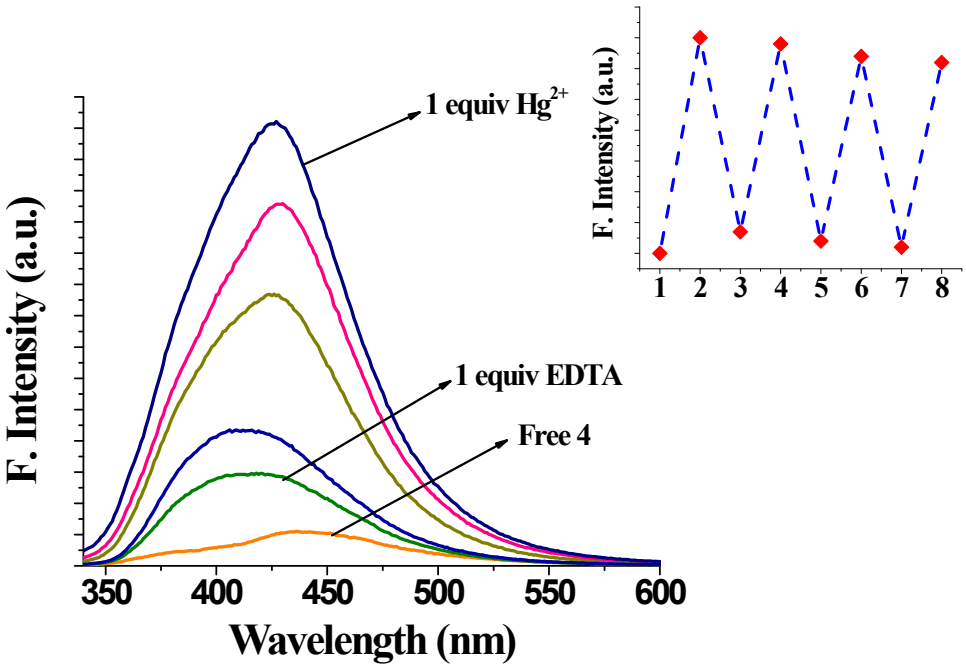

Fig. S14. Reversible interaction between **4** and EDTA by the introduction of Hg^{2+} to the system; Inset: Stepwise complexation/decomplexation cycles carried out with **4** and EDTA.

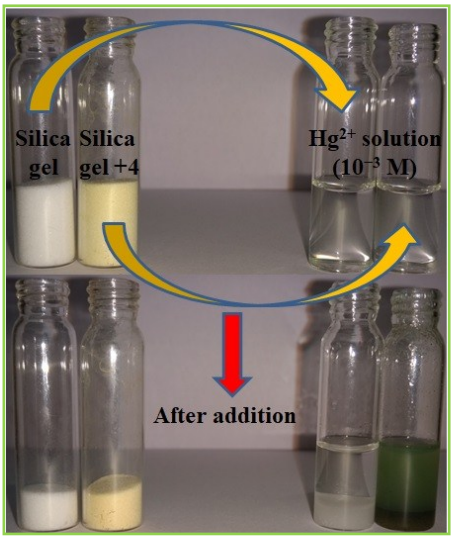

Fig. S15. Colour changes of silica gel soaked with **4** upon addition into aqueous solution of Hg^{2+} ion.

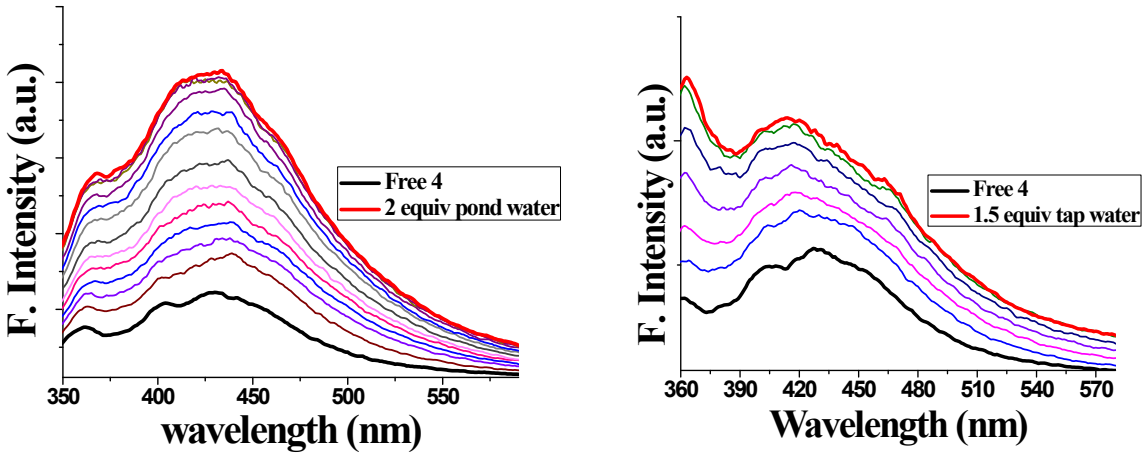

Fig. S16. Fluorescence emission titration of compound **4** (10^{-8} M) upon addition of (a) pond water and (b) tap water.

a)

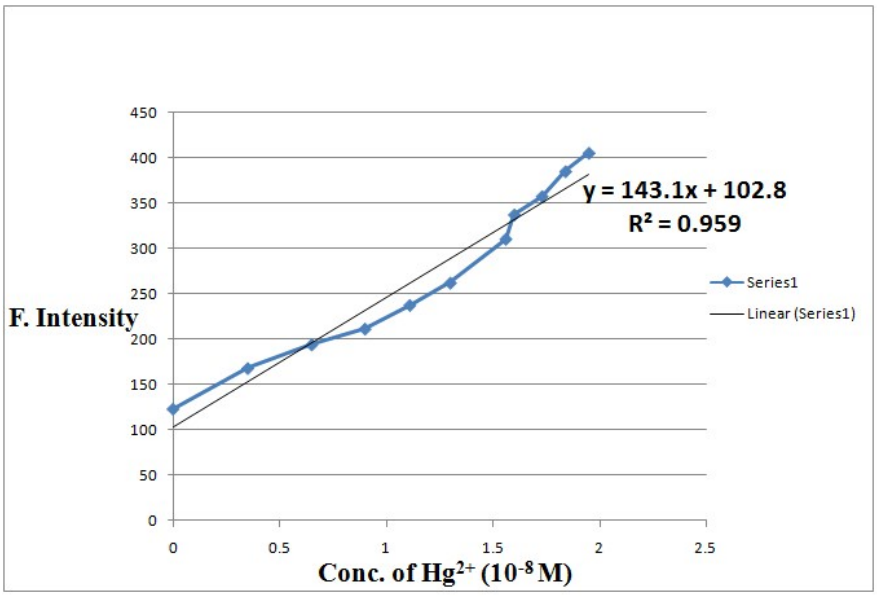

b)

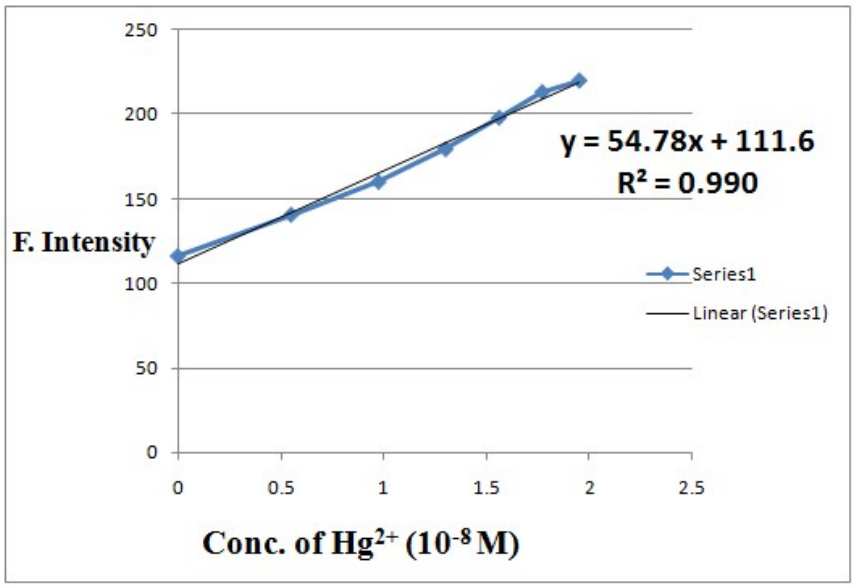

Fig. S17. Fluorescence calibration curve for (a) pond water and (b) tap water.

Table S1. Electron density, $\rho(r)$, Laplacian of electron density, $\nabla^2\rho(r)$, total energy density, H(r), potential energy density, V(r) and kinetic energy density, G(r) in hartree $Å^{-3}$ of selected bond critical points (BCPs) and cage critical point (CCP) in complex at the B3LYP/def2-SVP level of theory.

BCP/RCP	$\rho(r)$	$\nabla^2\rho(r)$	H(r)	V(r)	G(r)
N-Hg	0.116	0.377	-0.0327	-0.1588	0.126
	0.1161	0.3769	-0.0327	-0.1588	0.1261
O-Hg	0.0196	0.0658	0.00028	-0.0159	0.0161
	0.0196	0.0658	0.00028	-0.0158	0.01618

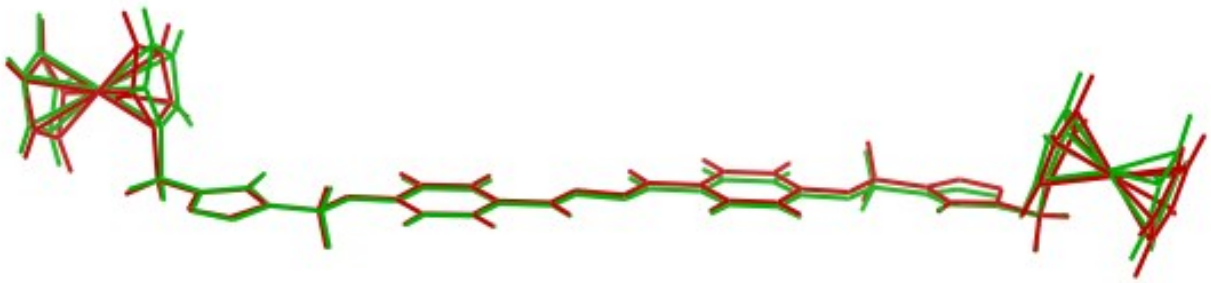

Fig. S18. Overlay structures of **4** optimized at S_0 state (Red) and S_1 state (Green).

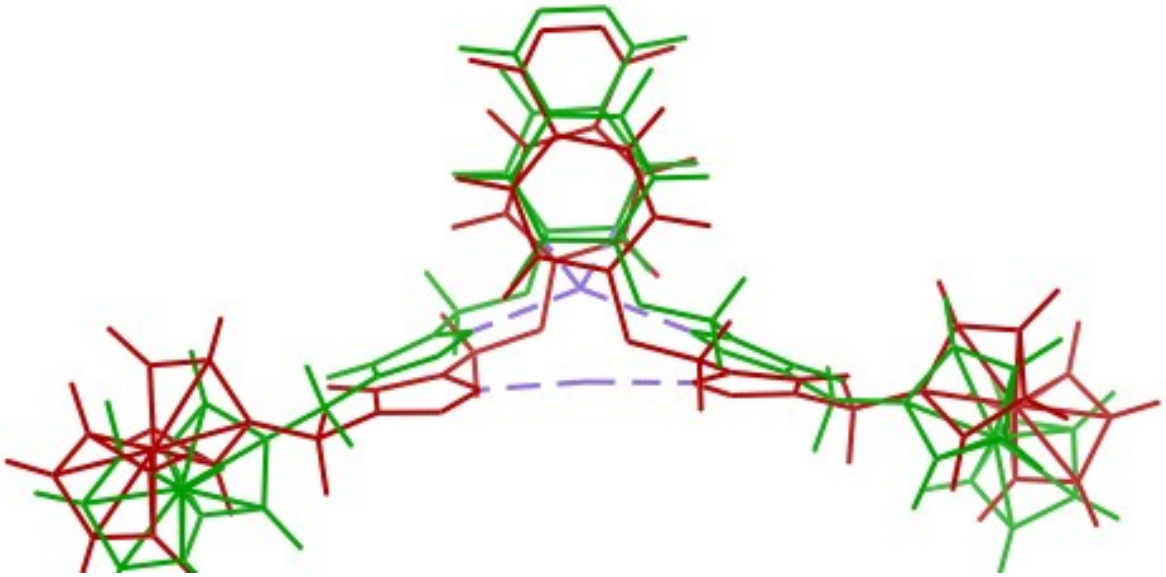

Fig. S19. Overlay structures of [**4**·Hg^{2+}] optimized at S_0 state (Red) and S_1 state (Green).